Geochemistry Geophysics Geosystems G3

Article
Volume 12, Number 8
10 August 2011
Q08006, doi:10.1029/2011GC003523
ISSN: 1525-2027

Published by AGU and the Geochemical Society

The provenance of sediments in the Gulf of Lions, western Mediterranean Sea

S. Révillon
UMR 6538, Domaines Océaniques, IUEM, Université de Bretagne Occidentale, F-29280 Plouzané, France

Ifremer, Département Géosciences Marines, F-29280 Plouzané, France (sidonie.revillon@univ-brest.fr)

G. Jouet and G. Bayon
Ifremer, Département Géosciences Marines, F-29280 Plouzané, France

M. Rabineau
UMR 6538, Domaines Océaniques, IUEM, Université de Bretagne Occidentale, F-29280 Plouzané, France

B. Dennielou
Ifremer, Département Géosciences Marines, F-29280 Plouzané, France

C. Hémond
UMR 6538, Domaines Océaniques, IUEM, Université de Bretagne Occidentale, F-29280 Plouzané, France

S. Berné
Ifremer, Département Géosciences Marines, F-29280 Plouzané, France

CEFREM, Université de Perpignan, F-66860 Perpignan, France

[1] In this study, we undertook a reconnaissance study of sediments provenance in the Gulf of Lions focusing over the last 16 ka. We used geochemical and isotopic tracers to determine the source of sediments and give insight into the weathering conditions prevailing. Sediments samples were selected both onshore and offshore from the western, eastern, and central part of the Gulf of Lions. We analyzed bulk sediments, coarse and fine silt, and clay fractions. Elemental and Nd isotope compositions appeared to differ from one grain size fraction to another one. These are interpreted in terms of zircon addition in the coarse silt fraction for the elemental concentrations and variable sources influences for the Nd isotope compositions. Our results indicate that sediments in the Gulf of Lions mainly originated from the Rhône River watershed although a contribution of Saharan dust is seen in one sample. Influence of Pyrenean small rivers is minor in these samples. Some Sr isotope compositions shifts are interpreted as reflecting variable amounts of chemical weathering that are consistent with published paleoclimatic reconstructions.

Components: 11,000 words, 7 figures, 4 tables.

Keywords: geochemistry; provenance; sediment; weathering.

Index Terms: 1030 Geochemistry: Geochemical cycles (0330); 4914 Paleoceanography: Continental climate records.

Received 20 January 2011; **Revised** 31 May 2011; **Accepted** 3 June 2011; **Published** 10 August 2011.

Révillon, S., G. Jouet, G. Bayon, M. Rabineau, B. Dennielou, C. Hémond, and S. Berné (2011), The provenance of sediments in the Gulf of Lions, western Mediterranean Sea, *Geochem. Geophys. Geosyst.*, *12*, Q08006, doi:10.1029/2011GC003523.

1. Introduction

[2] Studying sediment piles deposited and preserved in oceanic basins and continental margins provides an opportunity to examine how terrigenous sediments supply varied through time in relation to paleoenvironmental and climate changes [e.g., *Cole et al.*, 2009; *Colin et al.*, 2006; *Derry and France-Lanord*, 1996; *Galy et al.*, 2010; *Najman*, 2006]. In the past, most studies have focused on specific climatic zones where extreme climatic conditions prevailed such as cold glacial, tropical-monsoonal systems or mountainous areas [*Anderson et al.*, 1997; *Bickle et al.*, 2005; *Braun et al.*, 2005; *Colin et al.*, 2006; *Galy and France-Lanord*, 1999; *Revel et al.*, 2010; *Verplanck et al.*, 2009]. Conversely, temperate-dominated climatic zones have received less attention. The Mediterranean Sea is situated in a transitional climatic area and the influence of both high latitude (North Atlantic system) and low latitude (African subtropical monsoon system) have been investigated by previous studies [*Bout-Roumazeilles et al.*, 2007; *Naughton et al.*, 2009; *Popescu et al.*, 2010; *Sánchez Goñi et al.*, 2008].

[3] The elemental geochemistry of terrigenous sediments reflects a combination of multiple parameters such as provenance (source), chemical weathering, physical erosion or hydraulic sorting [*Taylor and McLennan*, 1985]. Numerous studies have demonstrated that the geochemical composition of sediments can be used as a powerful tool to determine their provenance [*Lee et al.*, 2008; *Mahoney*, 2005; *McLennan*, 1993; *Vital and Stattegger*, 2000, and reference therein]. Additionally, strontium (Sr) and neodymium (Nd) isotope compositions provide important information on the source areas as well as erosion and weathering conditions [e.g., *Cole et al.*, 2009; *Colin et al.*, 2006; *Derry and France-Lanord*, 1996; *Eisenhauer et al.*, 1999; *Grousset et al.*, 1998; *Revel-Rolland et al.*, 2005; *Tütken et al.*, 2002; *Verplanck et al.*, 2009].

[4] In this paper, we undertook a reconnaissance study of sediments provenance in the Gulf of Lions. We used geochemical and isotopic tracers to determine the source of sediments and give insight into the weathering conditions prevailing. These sediments were sampled from different geographic locations (eastern, central and western parts of the Gulf of Lion and in the terrestrial watersheds) but also at different ages during the last 16 ka Cal BP to examine the variability of sediment supply spatially and temporally.

2. Geological and Geochemical Background

2.1. The Gulf of Lions

[5] The Gulf of Lions is a siliciclastic passive margin located between the Pyrenean and Alpine orogenic belts in the northern part of the western Mediterranean Basin (Figure 1a). The development of the margin was initiated by an Oligo-Aquitanian rifting phase between the continent and the Corsica-Sardinia microplate, and the Burdigalian crustal opening [*Gueguen*, 1995; *Sioni*, 1997]. This margin is covered by sedimentary series dated from Oligocene to Quaternary [*Gorini et al.*, 1993]. The shelf is about 250 km long and 75 km wide. This shelf is relatively flat and dips gently seaward to the shelf break, located at a water depth between 120 and 150 m. The upper Pliocene-Quaternary deposits have recorded the sedimentary structures associated with glacial-interglacial sea level variations and significant subsidence at the shelf edge [*Lofi et al.*, 2003; *Rabineau et al.*, 2006]. This led to the deposition and preservation of various types of sedimentary bodies and to numerous canyons dissecting the continental slope [*Baztan et al.*, 2005; *Berné and Gorini*, 2005]. The Rhône River is supposed to be the main provider of sediments for the area, but depositional centers have moved across the margin concurrent with sea level changes. Indeed, the drainage patterns of the Rhône River varied through time depending on the exposure of the shelf during sea level lowstands. During the most recent post-glacial sea level rise, sediments were stored in prodeltas that form shelfal retrograding sediment bodies, still visible on the present seabed morphology [*Berné et al.*, 2007].

[6] The water circulation and sediment transport in the Gulf of Lions are mainly driven by the Northern or Liguro-Provençal current which follows the continental slope and also penetrates onto the shelf [*Millot*, 1999] (Figure 1a). On the shelf, a large amount of fine-grained sediment sourced from the Rhône is presently advected to the SW in response

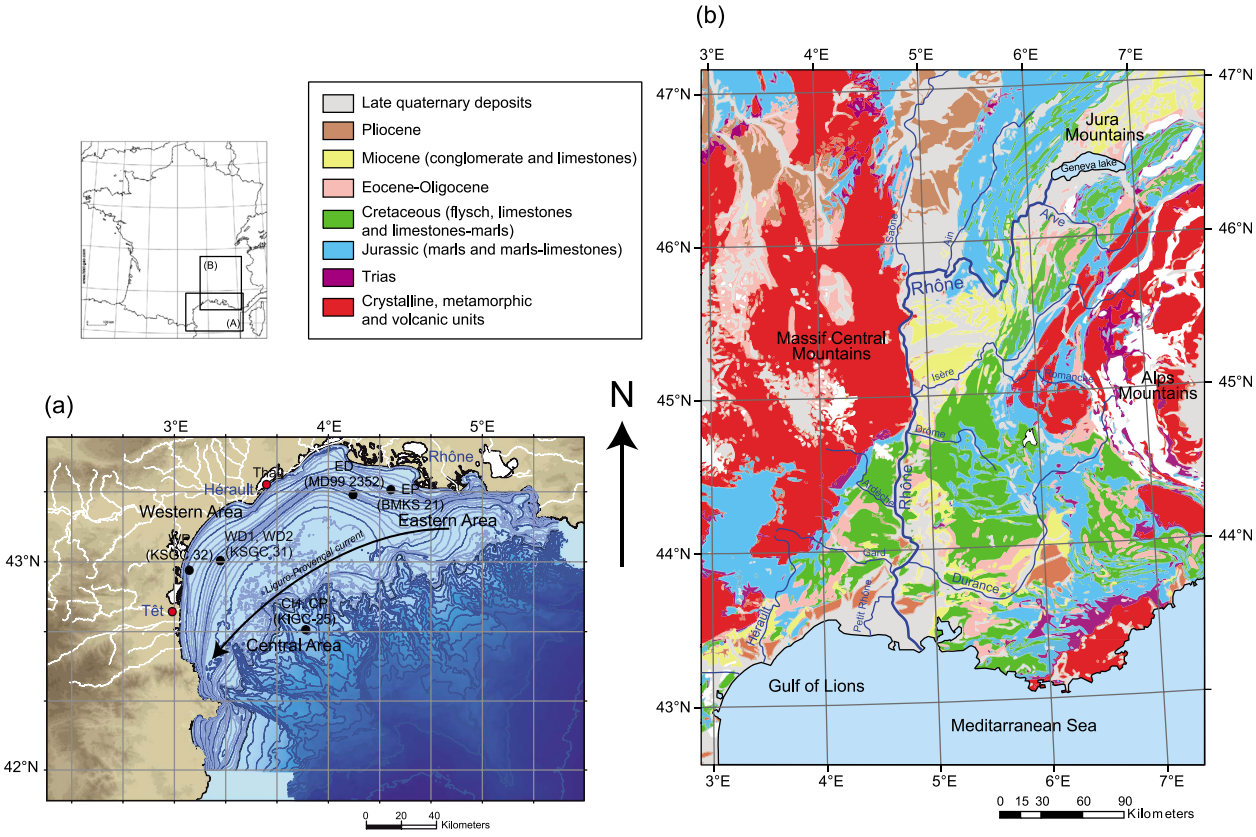

Figure 1

Figure 1. (a) Bathymetric map of the Gulf of Lions showing the studied marine sediment core locations and samples from potential source areas. (b) Geological map of the Rhône River drainage basin. The main lithologies are given in the legend in parenthesis.

to the dominant wind forcing [*Aloïsi*, 1986; *Dufois*, 2008].

2.2. The Rhône Watershed

[7] The Rhône River is 816 km long and has a drainage area of 98,800 km^2 (Figure 1b). Its hydrographic basin is largely characterized by mountainous catchments in the Alps, Massif Central, and Jura, inducing strong climatic heterogeneity encompassing oceanic, continental and Mediterranean rainfall regimes (Figure 1b). The geology of the Rhône watershed is complex due to the long Meso-Cenozoic tectonic activity of the area related to the opening and closing of the Tethys Sea and the overall convergence between Africa and Europe (Figure 1b). Nonetheless, three main lithological formation types are distinguished: the siliceous crystalline massifs mainly comprising granites (e.g., the Mont Blanc massif); sedimentary rocks of Cretaceous and Cenozoic ages consisting mainly of conglomerates, sandstones and limestones and finally sedimentary rocks of Jurassic ages consisting mainly of marls, black marls and limestones (Figure 1b). Within the main tributaries of the Rhône River, the drainage basins of both the Arve and Isère rivers encompass mainly crystalline and recent sedimentary formations. The Durance river watershed is different, comprising mostly older Jurassic black shales. Fluvioglacial deposits are widespread in the area and the Rhône River transports of lot of material that has been eroded from glaciers [*Ollivier et al.*, 2010]. The Rhône's catchment ends with a delta of 1455 km^2, which is the second largest in the Mediterranean Sea [*Pont et al.*, 2002].

2.3. Geochemical Background

[8] Multiple parameters must be taken into account when studying sediments geochemical compositions. Various geochemistry tools are used including, Rare Earth Elements (REE), immobile trace elements (i.e., Zr, Th, Sc …) and Nd isotope data for provenance studies, and more mobile trace elements (i.e., U, Cs …) and Sr isotope data to establish the

Table 1. Summary of Marine Sediment Cores and Samples Characteristics Used in This Study

Core	Latitude	Longitude	Water Depth (m)	Length (cm)	Depth Sampled (cm)	Location	Sublocation	Acronym Used in the Text	Calculated or Estimated Age (yr cal BP)
BMKS21	43°20.58 N	4°24.34 E	31	567	43	Eastern	Proximal	EP	1,712 ± 50
MD99-2352	43°19.15 N	4°09.64 E	70	1,540	1,510	Eastern	Distal	ED	14,606 ± 122
KIGC25	42°40.56 N	3°51.19 E	341	71	12	Central	Slope	CH	Holocene
KIGC25	42°40.56 N	3°51.19 E	341	71	70	Central	Slope	CP	Pleistocene
KSGC32	43°57.36 N	3°05.52 E	35	104	20	Western	Proximal	WP	1,415 ± 55
KSGC31	43°00.21 N	3°17.57 E	60	703	90	Western	Distal	WD1	974 ± 44
KSGC31	43°00.21 N	3°17.57 E	60	703	671	Western	Distal	WD2	8,940 ± 76

alteration conditions in which sediments were formed.

[9] Since early studies, in the 1980s, it has been demonstrated that Nd isotope compositions are robust indicators of sediment provenance [*Goldstein and O'Nions*, 1981; *Grousset et al.*, 1988; *White et al.*, 1985] and that they are not modified through sedimentary processes such as erosion/weathering. Samarium (Sm) and Nd behave consistently and little or no fractionation occurs during the sedimentary cycle [*Goldstein et al.*, 1984; *Grousset et al.*, 1988; *Mahoney*, 2005; *Taylor and McLennan*, 1985]. Although, it is often assumed that there is no significant dependence of Sm-Nd isotope ratios on grain size [*Tütken et al.*, 2002], such features have already been reported [*Derry and France-Lanord*, 1996; *Innocent et al.*, 2000].

[10] Strontium isotope compositions can also be used in sediment provenance studies as the $^{87}Sr/^{86}Sr$ ratio of sediment is a function of the Sr isotope composition of the original eroded lithology. It is also well established that the radioactive decay of ^{87}Rb to ^{87}Sr will impart various $^{87}Sr/^{86}Sr$ to geological material and minerals, depending on their original Rb/Sr ratio and elapsed time since formation. For example, micas, such as biotite have elevated $^{87}Sr/^{86}Sr$ whereas plagioclase, a low Rb/Sr mineral, has lower $^{87}Sr/^{86}Sr$. The original Sr isotope composition of sediment therefore depends on the relative proportions of each mineral. In many recent studies, the large variations observed in the $^{87}Sr/^{86}Sr$ of marine sediments have been attributed to various degree of chemical weathering on the continent [*Cole et al.*, 2009; *Colin et al.*, 2006; *Jung et al.*, 2004]. During chemical weathering, the radiogenic Sr is preferentially released to the fluid, due to the early breakdown of mica (e.g., mainly biotite) and K-feldspar which are both minerals with high $^{87}Sr/^{86}Sr$ [*Blum and Erel*, 1997; *Bullen et al.*, 1997; *Jeong et al.*, 2006; *Taylor et al.*, 2000]. Consequently, the $^{87}Sr/^{86}Sr$ of sediment is lowered [*Blum and Erel*, 1997; *Jeong et al.*, 2006]. However, it must also be noticed that such an evolution critically depends on the amount of altered biotite. If the proportion of altered radiogenic minerals is low, the effect on bulk sediment Sr isotope composition will be small [*Pett-Ridge et al.*, 2009].

3. Methods

3.1. Cores and Samples Descriptions

[11] The main characteristics of the cores and studied samples are listed in Table 1. Radiocarbon ages used to construct age-depth relationships and calculated ages for our samples are reported in Table 2.

[12] Core MD99-2352 was collected with the "Calypso" piston corer of R/V *Marion Dufresne* on the inner shelf. It is mainly composed of brown silts with intercalated silty-sandy levels [*Berné et al.*, 2007]. Two coarse layers are present at 1 m and at the base of the core [*Berné et al.*, 2007]. One sample was taken from this core at 1510 cm depth. An age-depth relationship was established, based on 14 radiocarbon dates distributed along the core. A linear regression calculation was used to calculate an age of 14606 ± 122 yr cal BP for our sample (Tables 1 and 2) following the model published by *Berné et al.* [2007]. Core BMKS-21 was recovered during Beachmed cruise on R/V *Le Suroît* on the inner shelf. It is mainly composed of dark clays and alternating clay, clayey-silt and silt levels. An age-depth relationship was established, based on 7 radiocarbon dates distributed along the core. One sample was taken for our study at 43 cm and the age of the sample is calculated at 1712 ± 50 yr cal BP (Tables 1 and 2).

[13] Cores KSGC-31, KSGC-32 and KIGC-25 were collected during GMO2-CARNAC cruise on R/V *Le Suroît*. Both KSGC-31 and KSGC-32 cores were collected on the inner shelf and KIGC-25 was collected on the slope. Core KSGC-31

Table 2. Compilation of ^{14}C Dates Used in This Study[a]

Core	Sample Depth (cm)	Sample Weight (mg)	Dated Material	Sample Number	Conventional C^{14} Age (BP)	1 σ Calibrated Age (y BP)	Probability Distribution
BMKS-21	20–23	151	*Turritella* sp.	Poz-11198	2,050 ± 30	1,573–1,673	1.000
	111–113	60	Sediment >63 μm with vegetal debris	Poz-11459	2,040 ± 35	1,946–2,046	1.000
	220–222	166	Sediment >63 μm with vegetal debris	Poz-11461	2,245 ± 35	2,179–2,241 2,302–2,334	0.64–0.33
	337–339C	25	Sediment >63 μm with vegetal debris	Poz-11377	2,060 ± 30	1,988–2,062 2,086–2,104	0.85–0.13
	337–339T	376	*Turritella* sp.	Poz-11199	2,120 ± 30	1,659–1,767	1.000
	445–446	4.3	*Turritella* sp.	Poz-11200	2,135 ± 30	1,683–1,781	1.000
	553–555	153	Sediment >63 μm with vegetal debris	Poz-11462	2,480 ± 40	2,058–2,206	1.000
MD99-2352	123	340	*Acanthocardia echinata*	LLNL-95846	4,955 ± 45	5,249–5,362 25,367–5,388	0.91–0.099
	286	109	*Nucula* sp. (nucleus)	Poz-3842	9,890 ± 60	10,661–10,925	1.000
	401–403	9.6	*Turitella* communis	Poz-3843	10,000 ± 50	10,909–11,110	1.000
	519–521	10.7	Mixed benthic forams bivalves, gastropods andostracods	Poz-3844	10,070 ± 60	10,949–10,953 11,019–11,177	0.011–0.99
	731	59	*Turitella* communis	Poz-3845	10,310 ± 50	11,216–11,333	1.000
	799–801	15.3	Mixed benthic forams bivalves, gastropods andostracods	Poz-3846	11,320 ± 60	12,845–12,908	1.000
	928–932	19.2	*Corbula gibba*	Poz-3848	10,590 ± 50	11,738–11,954	1.000
	948	105	*Corbula gibba*	LLNL-95847	10,475 ± 40	11,409–11,523 11,560–11,718	0.41–0.59
	1,105–1,107	19.6	Mixed benthic forams bivalves, gastropods andostracods	Poz-3849	11,340 ± 50	12,856–12,913	1.000
	1,305–1,307	42.6	*Ammonia beccarii* or *Elphidium crispum* bivalvia	Poz-3850	11,820 ± 50	13,225–13,317	1.000
	1,393	31	*Corbula gibba*	LLNL-95848	11,840 ± 40	13,244–13,326	1.000
	1,494	64	*Turitella* communis.	LLNL-95849	12,855 ± 40	14,280–14,648	1.000
	1,505	290	*Mya truncata*	LLNL-95850	13,245 ± 40	15,031–15,258	1.000
	1,534–1,536	35.7	*Mytilus* sp.	LLNL-98908	13,090 ± 50	14,870–15,111	1.000
KSGC31	41	28	*Pecten* sp.	Poz-15009	700 ± 30	298–385	1.000
	480–482	1,244	*Ostrea* sp.	Poz-14007	5,955 ± 35	6,311–6,400	1.000
	501–502	26	*Turitella* sp.	Poz-14008	6,380 ± 40	6,789–6,907	1.000
	700–702	74	*Turitella* sp.	Poz-15010	9,190 ± 50	9,920–10,106	1.000
KSGC32	68–70	85	*Pecten* sp.	Poz-14009	2,040 ± 35	1,555–1,662	1.000

[a]Dates obtained on cores BMKS21 and MD99-2352 have already been published by *Berné et al.* [2007] and *Beaudouin et al.* [2007]. Absolute dates were obtained with accelerator mass spectrometer (AMS) ^{14}C dating of well-preserved shells and microfauna. They were made at Lawrence Livermore National Laboratory (LLNL) and at Poznan Radiocarbon Laboratory (PRL). The ages reported herein are delta ^{13}C-normalized conventional ^{14}C years. For ages between 0 and 21,880 yr ^{14}C BP, calendar (i.e., calibrated) ages were calculated using the Calib 5.0 sofware [*Stuiver and Reimer*, 1993]. For marine material, the Marine04 calibration curve [*Hughen et al.*, 2004] was used with no deviation from the average reservoir age (−408 years). For continental material the Intcal04 calibration curve was used [*Reimer et al.*, 2004].

consists of dark to gray clays and thin silty levels by the bottom of the core. Two samples were taken and four radiocarbon dates are available. The ages and uncertainties of the analyzed sediments are estimated thanks to the absolute radiocarbon dates directly surrounding the samples; the estimates ages are 974 ± 44 yr cal BP and 8940 ± 76 yr cal BP, respectively (Tables 1 and 2). Core KSGC-32 consists of alternating levels of fine sand, silt and clays with a large interval of homogeneous dark-olive clays between 12 cm and 47 cm. One sample was taken from this core at 20cm depth (Table 1). Only one radiocarbon date is available for this core and the age of the sample was calculated using a linear regression between this date and the estimated age of a seismic discontinuity at 110 cm on the Core KSGC-32 also sampled seaward in Core KSGC-31. The seismic discontinuity D601 is sampled in KSGC-31 at 150 cm with an estimated age of 1800 yr cal BP based on the age model constrained by 4 absolute radiocarbon dates [*Jouet*, 2007]. The resulting age of the sample is 1415 ± 55 yr cal BP (Tables 1 and 2). Core KIGC-25 is a short core composed of clays and two samples were taken. No radiocarbon dates are available for this core. However, based on sedimentological criteria (color changes) and comparison with similar dated cores it is possible to suggest a time interval for the deposition of these two samples. Hence, sample KIGC-25-12 should be Holocene in age (based on the light color of sediments) and sample KIGC-25-70 should be late Pleistocene in age (Table 1). A former gravity piston core at the same location (age model of MD99-2348 available in the work by *Sierro et al.* [2009]) confirms an age of 16382–16791 yr cal BP at 80 cm.

[14] In addition to marine sediments cores, we studied samples from some terrestrial watersheds. One sample originates from the river Têt (Perpignan city, Figure 1a), five samples originate from a surface sediment core recovered in the Thau lagoon (Figure 1a) and 2 samples were recovered along the Durance River within the Jurassic black marls ("marnes noires de Haute Provence") (Figure 1b). These results were used, together with published data in the area [*Arnaud et al.*, 2008; *Henry*, 1994; *Henry et al.*, 1997; *Revel-Rolland et al.*, 2005; *Révillon et al.*, 2008].

3.2. Analytical Techniques

[15] All sediment samples were sieved at 63 μm and only the fraction <63 μm was retained for further geochemical analyses. An aliquot of this fraction was taken as a "bulk" sample (<63 μm). The remaining was separated into three distinct fractions: clays (<2 μm); fine silts (2–20 μm) and coarse silts (20–63 μm). The clay fraction was separated by centrifugation. The 2–20 μm fraction was separated from the 20–63 μm one by decantation.

[16] Each fraction was chemically treated to remove organic matter, authigenic Fe-Ti oxides and carbonates in order to analyze only the siliciclastic components of the terrigenous material. The procedure included three leaching steps with H_2O_2, acetic acid and HNO_3 and is described in details by *Bayon et al.* [2002]. About 100 mg of the various sediment fractions were weighted and dissolved in high pressure Teflon bombs in a mixture of HF, HNO_3 and $HClO_4$ following the method described by *Révillon and Hureau-Mazaudier* [2009].

[17] Trace elements were measured by HR-ICP-MS (Element 2) at the Pôle de Spectrométrie Océan (PSO, UBO/CNRS/Ifremer, Brest, France). Here 900 μl of solution were carefully weighted and mixed with 70 μl of Tm spike prior to dilution in HNO_3 2% following the method described by *Barrat et al.* [1996] and *Bayon et al.* [2009]. Sr and Nd fractions were chemically separated using the Eichrom specific resins TRU-spec, Sr-spec and Ln-spec following usual procedures [*Pin and Santos Zalduegui*, 1997].

[18] Sr and Nd isotope compositions were measured either in dynamic mode on a Finnigan MAT 261 or in static mode on a Finnigan TRITON at the PSO. Procedural blanks were <300 pg and therefore negligible in all cases. Sr isotope compositions of standard solution NBS987 gave $^{87}Sr/^{86}Sr$ = 0.710267 ± 0.000006 (2σ, n = 78) and Nd isotope compositions of standard solutions La Jolla and JNdi gave $^{143}Nd/^{144}Nd$ = 0.512849 ± 0.000008 (2σ, n = 29) and $^{143}Nd/^{144}Nd$ = 0.512100 ± 0.000006 (2σ, n = 21), respectively; $^{143}Nd/^{144}Nd$ is normalized to $^{146}Nd/^{144}Nd$ = 0.7219. For convenience, Nd isotope results are expressed as: $\varepsilon_{Nd0} = [(^{143}Nd/^{144}Nd_{(meas)}/^{143}Nd/^{144}Nd_{(CHUR)})-1]*10^4$. The CHUR (Chondritic Uniform Reservoir) value is 0.512638 [*Jacobsen and Wasserburg*, 1980].

4. Results

4.1. Trace Element Data

[19] Trace element concentrations of marine sediments and terrestrial samples are presented in Tables 3 and 4, respectively. The REE patterns normalized to UCC (Upper Continental Crust

Table 3. Trace Element Concentrations (ppm) and Sr and Nd Isotope Compositions of Gulf of Lions Samples

	KSGC32-20				KIGC25-12				KIGC25-70				KSGC31-90			
	<63 μm	20–63 μm	2–20 μm	<2 μm	<63 μm	20–63 μm	2–20 μm	<2 μm	<63 μm	20–63 μm	2–20 μm	<2 μm	<63 μm	20–63 μm	2–20 μm	<2 μm
Cs	20.3	6.31	18.7	22.8	12.1	5.51	13.1	19.4	8.67	4.50	13.7	39.6	15.2	6.71	12.4	32.9
Rb	142	72.8	91.2	187	90.7	72.4	82.3	94.5	61.1	60.1	157	129	180	104	92.3	116
Ba	402	235	465	313	200	300	273	123	166	273	363	382	504	366	295	440
Th	10.4	6.41	10.3	8.92	5.4	7.6	4.6	2.7	3.29	4.94	9.53	4.45	11.3	7.41	5.23	6.97
U	3.31	2.80	3.76	2.59	1.66	2.57	2.20	0.90	1.12	2.00	2.95	2.39	2.78	2.35	2.44	2.85
Nb	18.4	23.7	61.0	19.3	13.8	16.0	29.6	10.9	12.8	9.44	35.7	40.9	29.5	23.6	31.2	46.2
Ta		1.60	4.16	1.29	1.08	1.15	1.71	0.47	0.85	0.58	2.11	2.40	1.91	1.40	1.98	2.71
La	34.1	22.9	36.4	27.0	17.0	24.8	19.2	9.1	12.3	18.5	35.2	27.3	38.0	22.7	20.6	23.1
Ce	66.0	52.1	81.9	44.8	41.5	52.6	56.5	20.4	32.6	44.3	66.3	32.8	64.8	51.6	67.3	39.2
Pr	7.38	5.08	10.02	5.37	3.51	5.81	4.24	1.78	2.61	4.17	7.28	5.39	8.49	4.88	4.59	5.20
Sr	109	74.2	102	97.9	66.6	89.3	102	42.8	45.1	64.6	114	87.4	127	96	123	102
Nd	26.5	19.5	32.6	18.9	12.3	21.4	14.2	6.04	9.34	15.1	25.3	19.4	27.7	17.1	15.1	18.8
Zr	221	344	353	115	153	211	178	106	165	214	184	188	173	183	182	184
Hf		10.1	9.33	3.37	4.46	5.68	4.51	3.09	4.57	5.80	5.05	5.10	4.97	4.98	5.02	5.06
Sm	4.63	3.51	6.63	3.02	2.03	4.02	2.10	0.85	1.55	2.66	3.96	2.71	4.79	3.11	2.57	3.02
Eu	0.83	0.58	0.98	0.53	0.36	0.70	0.40	0.15	0.26	0.43	0.66	0.45	0.73	0.53	0.38	0.53
Gd	3.94	2.89	4.56	2.23	1.65	3.49	1.41	0.61	1.22	2.14	3.01	1.45	3.11	2.52	1.87	1.89
Tb	0.63	0.45	0.80	0.34	0.26	0.56	0.29	0.09	0.19	0.29	0.47	0.21	0.55	0.45	0.30	0.32
Dy	3.86	2.49	4.28	2.06	1.69	3.41	1.91	0.62	1.19	1.52	2.96	1.72	3.14	2.61	1.64	2.07
Y	24.8	14.6	24.1	12.3	10.0	20.6	10.7	3.76	7.34	7.73	17.5	9.53	19.9	16.9	11.0	10.7
Ho	0.84	0.53	0.94	0.47	0.37	0.72	0.42	0.14	0.27	0.29	0.63	0.39	0.71	0.53	0.40	0.49
Er	2.58	1.53	3.10	1.40	1.19	2.15	1.33	0.48	0.88	0.79	1.95	1.21	2.42	1.79	1.27	1.52
Yb	2.66	1.72	2.65	1.58	1.32	2.19	1.54	0.58	1.01	0.76	2.12	1.49	2.29	1.75	1.29	1.84
Lu	0.37	0.24	0.45	0.24	0.19	0.31	0.22	0.08	0.15	0.10	0.31	0.20	0.37	0.26	0.21	0.26
Sc	12.7	6.33	13.9	14.3	7.45	7.62	11.2	6.99	4.86	4.11	12.7	11.9	14.8	9.38	9.52	15.2
Ti	0.92	1.01	1.98	0.68	0.69	0.67	0.95	0.63	0.63	0.51	1.19	1.25	0.92	0.75	1.03	1.33
V	117	75.9	229	178	103	41.0	116	152	81.1	39.8	150	382	136	86.5	121	304
Cr	52.9	55.7	239	146	15.3	4.60	32.8	16.2	7.93	3.68	145		92.3	145	98.4	431
Mn	179	162	323	169	186	201	221	158	148	171	248	198	181	194	209	214
Co	7.60	6.42	17.83	12.07	9.05	6.45	9.90	11.4	5.71	4.76	10.8	15.2	7.82	6.09	7.74	15.9
Ni	20.6	23.9	79.9	56.3	52.2	32.8	64.0	77.8	38.2	29.2	66.1	98.7	46.3	33.9	52.0	90.3
Cu	12.9	11.1	31.6	23.8	14.5	6.56	15.48	22.3	6.01	3.47	15.3	16.5	9.71	5.26	9.84	27.2
Ga	19.7	12.7	37.8	30.9	18.7	12.4	20.8	27.1	16.4	11.5	22.5	59.4	21.9	16.1	20.6	47.7
Zn	152	75.3	237	121	75.9	55.5	108	81.3	50.3	45.5	100	109	202	81.4	184	213
$^{87}Sr/^{86}Sr$	0.721960	0.721460	0.722399	0.721801	0.719376	0.718640	0.719379	0.719588	0.718716	0.717998	0.719324	0.718555	0.718699	0.719506	0.719050	0.718099
2σ e	0.000002	0.000007	0.000005	0.000003	0.000004	0.000005	0.000010	0.000004	0.000006	0.000006	0.000003	0.000003	0.000003	0.000005	0.000003	0.000003
$^{143}Nd/^{144}Nd$	0.512044	0.512065	0.512021	0.512007	0.512071	0.512109	0.512056	0.512065	0.512092	0.512101	0.512084	0.512059	0.512072	0.512092		0.512051
2σ e	0.000004	0.000001	0.000002	0.000009	0.000002	0.000004	0.000005	0.000004	0.000006	0.000003	0.000007	0.000002	0.000003	0.000002		0.000002
εNd_0	−11.6	−11.2	−12.0	−12.3	−11.1	−10.3	−11.4	−11.2	−10.7	−10.5	−10.8	−11.3	−11.0	−10.7		−11.5

Table 3. (continued)

	KSGC31-671				BMKS21-43				MD99-2352-1510			
	<63 μm	20–63 μm	2–20 μm	<2 μm	<63 μm	20–63 μm	2–20 μm	<2 μm	<63 μm	20–63 μm	2–20 μm	<2 μm
Cs	13.1	5.57	8.98	25.5	10.0	4.85	14.3	45.0	18.6	6.00	14.6	22.2
Rb	82.6	66.1	86.8	125	107	70.1	138.6	158.3	73.1	91.1	113	224
Ba	273	285	334	192	287	243	317	440	287	302	282	481
Th	4.54	5.27	6.21	2.95	7.54	6.32	7.35	6.07	6.58	6.46	6.05	7.38
U	2.25	2.13	2.29	1.07	2.65	2.35	2.53	3.05	3.25	2.29	2.84	2.30
Nb	29.5	11.8	17.8	16.7	24.0	23.0	30.7	58.0	50.2	17.0	31.7	18.8
Ta	1.69	0.71	1.07	0.65	1.59	1.46	2.10	3.58	3.08	1.10	2.17	0.96
La	19.5	19.2	21.7	11.6	28.3	21.9	29.0	30.0	39.9	21.3	25.0	29.3
Ce	56.8	44.4	48.3	22.0	58.5	54.5	55.0	39.1	55.7	42.1	72.0	53.8
Pr	4.25	4.17	4.82	2.20	6.19	5.15	6.20	6.41	8.09	4.67	4.92	5.65
Sr	101	86.0	96.8	60.5	99.6	79.3	107	88.6	107	75.2	112	121
Nd	14.3	14.8	17.2	7.39	21.9	18.1	22.3	22.8	29.8	17.0	16.6	19.1
Zr	178	178	148	130	274	370	186	235	276	175	175	98.7
Hf	4.45	4.82	4.19	3.69	7.51	9.56	5.06	6.34	7.70	4.83	4.84	2.89
Sm	2.07	2.48	2.73	1.00	3.65	3.42	3.46	3.53	4.18	2.78	2.61	2.51
Eu	0.40	0.41	0.46	0.16	0.54	0.49	0.55	0.58	0.74	0.46	0.40	0.40
Gd	1.41	1.91	2.14	0.64	2.80	2.88	2.58	1.97	2.57	1.90	1.61	1.14
Tb	0.30	0.28	0.35	0.10	0.42	0.41	0.40	0.30	0.39	0.36	0.25	0.21
Dy	1.92	1.64	2.20	0.68	2.53	2.57	2.45	2.02	2.58	2.31	1.57	1.48
Y	10.8	10.8	13.2	4.78	15.5	16.3	14.9	10.5	14.5	14.1	10.1	9.24
Ho	0.41	0.34	0.49	0.17	0.55	0.50	0.52	0.51	0.59	0.50	0.40	0.35
Er	1.33	1.07	1.55	0.61	1.62	1.48	1.59	1.57	1.65	1.52	1.25	1.21
Yb	1.52	1.24	1.65	0.78	1.80	1.59	1.71	1.92	2.08	1.69	1.39	1.39
Lu	0.22	0.18	0.24	0.12	0.26	0.24	0.25	0.29	0.30	0.24	0.21	0.21
Sc	11.3	6.32	9.04	7.18	8.62	5.52	10.3	14.0	9.66	7.48	9.72	13.9
Ti	0.96	0.56	0.80	0.73	0.92	0.79	1.15	1.67	1.62	0.58	1.01	0.62
V	116	55.9	82.3	208	105	69.4	130	385	222	74.1	149	186
Cr	32.9	6.47	15.4	12.0	108	53.0	123	447	284	65.7	117	101
Mn	224	152	158	103	162	170	169	175	232	181	171	117
Co	10.0	4.42	5.46	6.86	4.74	4.01	5.89	12.7	11.0	4.91	6.48	6.38
Ni	64.2	33.6	43.1	47.6	40.2	28.6	46.7	92.7	86.8	44.3	55.8	46.4
Cu	15.7	2.37	3.39	7.89	3.78	3.07	5.44	14.4	10.5	5.44	5.81	7.72
Ga	21.0	13.9	17.8	33.0	17.4	14.1	23.3	63.2	36.4	14.0	23.3	28.2
Zn	109	56.8	71.7	53.8	101	47.0	80.1	122	105			41.3
$^{87}Sr/^{86}Sr$	0.717168	0.717200	0.717348	0.716921	0.718498	0.718500	0.718613	0.717548	0.719334	0.719796	0.719147	0.719403
2σ e	0.000004	0.000003	0.000003	0.000003	0.000009	0.000007	0.000005	0.000003	0.000003	0.000003	0.000003	0.000003
$^{143}Nd/^{144}Nd$	0.512095	0.512095	0.512074	0.512059	0.512086	0.512136	0.512057	0.512048	0.512067	0.512108	0.512056	0.512059
2σ e	0.000005	0.000002	0.000002	0.000003	0.000002	0.000011	0.000013	0.000002	0.000004	0.000014	0.000003	0.000003
εNd_0	−10.6	−10.6	−11.0	−11.3	−10.8	−9.8	−11.3	−11.5	−11.1	−10.3	−11.4	−11.3

Table 4. Trace Element (ppm) and Sr and Nd Isotope Compositions of Terrestrial Samples

				Thau Lagoon				
Sample	Têt	Durance 1	Durance 2	T11H13	T11H23	T11H33	T11H39	T11H39*
Cs	8.03	13.1	14.3	15.4	14.7	12.9	10.5	14.3
Rb	142.9	129.0	141.7	144.5	156.0	146.2	140.1	166.4
Ba	511.5	351.3	394.0	378.3	386.7	348.2	335.9	360.5
Th	14.3	11.1	11.1	10.4	10.5	9.8	10.2	10.5
U	3.33	2.70	2.28	3.14	3.65	2.99	2.86	3.02
Nb	18.7	18.7	17.0	13.2	10.5	14.1	10.3	15.7
Ta	1.7	1.3	1.6	1.0	0.9	2.4	0.8	1.1
La	41.5	40.4	33.6	29.7	30.2	30.6	30.7	33.0
Ce	82.7	74.9	67.3	57.2	56.9	59.4	58.6	63.8
Pb	56.8	23.9	55.8	105.1	94.0	54.5	45.8	44.2
Pr	9.89	8.86	7.14	6.56	6.61	6.73	6.87	7.18
Sr	78.4	306.9	63.6	89.9	95.7	90.2	95.1	96.1
Nd	36.9	30.7	25.0	23.8	24.0	24.6	24.9	26.0
Zr	166	164	159	116	119	134	103	137
Hf	4.5	4.2	3.9	2.8	3.0	3.4	2.7	3.4
Sm	7.34	4.60	4.02	4.29	4.33	4.34	4.41	4.58
Eu	1.23	0.79	0.71	0.75	0.78	0.78	0.78	0.82
Ti	0.76	0.90	0.75	0.68	0.54	0.65	0.54	0.71
Gd	6.63	3.24	3.10	3.32	3.44	3.44	3.52	3.73
Tb	1.07	0.51	0.55	0.55	0.56	0.55	0.57	0.59
Dy	6.57	3.10	3.60	3.34	3.42	3.39	3.38	3.54
Y	41.3	18.2	24.8	21.5	22.0	21.5	21.2	23.0
Ho	1.35	0.64	0.77	0.69	0.71	0.70	0.69	0.75
Er	3.83	1.87	2.27	2.02	2.07	2.03	1.99	2.16
Yb	3.57	1.86	2.18	1.98	2.03	1.97	1.99	2.12
Lu	0.51	0.26	0.31	0.28	0.29	0.29	0.28	0.31
Sc	13.4	13.7	14.5	13.4	13.9	13.2	14.7	14.5
V	72.4	138.0	147.9	96.7	95.0	95.3	96.3	98.2
Cr	57.6	91.6	77.1	57.8	60.7	42.2	72.8	34.5
Mn	453	120	961	213	294	212	277	222
Co	9.6	11.9	37.9	11.0	11.9	9.9	9.5	9.1
Ni	26.3	81.8	120.3	46.0	49.6	44.8	46.8	46.1
Cu	29.4	29.2	71.5	139	133	127	252	406
Ga	21.3	23.2	20.6	19.8	20.4	19.8	20.9	20.5
Zn	120	133	120	560	303	371	154	172
$^{87}Sr/^{86}Sr$	0.731032	0.711343	0.722783	0.719010	0.719165	0.720284	0.719900	0.720177
2σ e	0.000003	0.000003	0.000003	0.000003	0.000003	0.000006	0.000003	0.000005
$^{143}Nd/^{144}Nd$	0.512095	0.511992	0.512045	0.512082	0.512084	0.512064	0.512067	0.512079
2σ e	0.000002	0.000003	0.000004	0.000003	0.000006	0.000006	0.000003	0.000006
εNd_0	−10.6	−12.6	−11.5	−10.8	−10.8	−11.2	−11.1	−10.9

[*Taylor and McLennan*, 1995]) (Figures 2a and 2b) of bulk samples (<63 μm fraction) are relatively homogeneous. They are almost flat, consistent with an origin from erosion of continental material [*McLennan*, 1993]. They also show that the Pleistocene sample from the Central area (CP, KIGC-25-70, Figure 2a) displays the lowest REE content (0.4*UCC). One distal (WD1, KSGC-31-90) sample and the proximal sample from the western area (WP, KSGC-32-20, Figure 2a) display concentration in REE similar to UCC. REE patterns of the fine silts (2–20 μm fractions) are almost flat and very similar to the bulk samples REE patterns. One exception to this is sample WP which displays higher concentrations compared to UCC. REE patterns of the coarse silts (20–63 μm fractions) are characterized by very homogeneous Light Rare Earth Element (LREE) concentrations and more heterogeneous Heavy Rare Earth Element (HREE) patterns. All samples show LREE content at about UCC values while HREE contents are more variable with HREE depleted pattern (CP), flat HREE pattern in the proximal sample from the eastern area (EP, BMKS-21-43, Figure 2a) to enriched HREE patterns (remaining of the samples). The clay fraction (<2 μm) displays the lowest REE contents with concave patterns illustrating slight depletion of the Middle Rare Earth Element (MREE) compared to the LREE and HREE (Figure 2a). REE patterns of terrestrial samples (<63 μm fraction) are very homogeneous presenting flat patterns very close to continental crust (Figure 2b). They are also highly

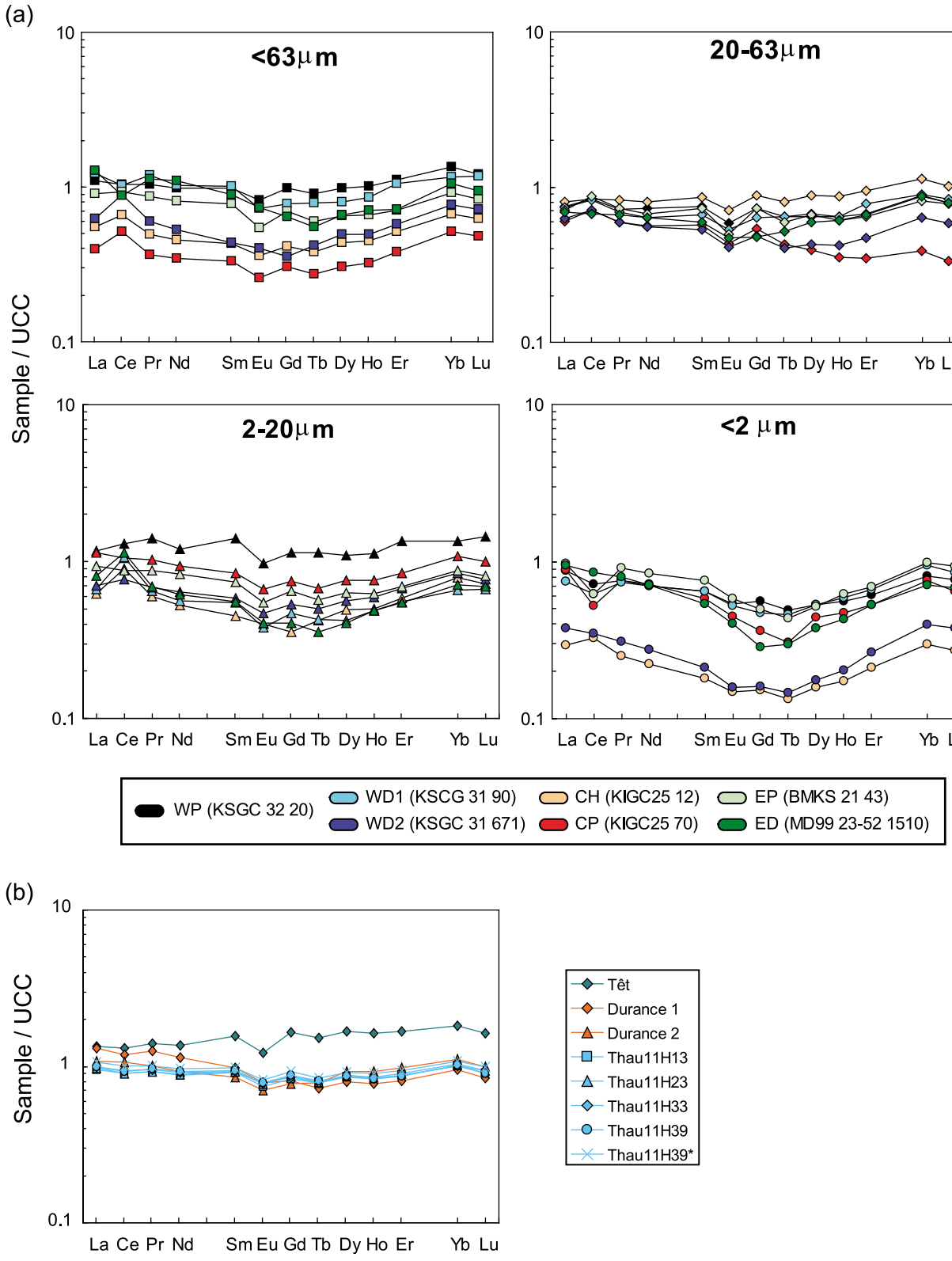

Figure 2. (a) REE patterns, normalized to UCC, of the various grain size fractions of marine sediment cores samples. (b) REE patterns, normalized to UCC, of terrestrial samples.

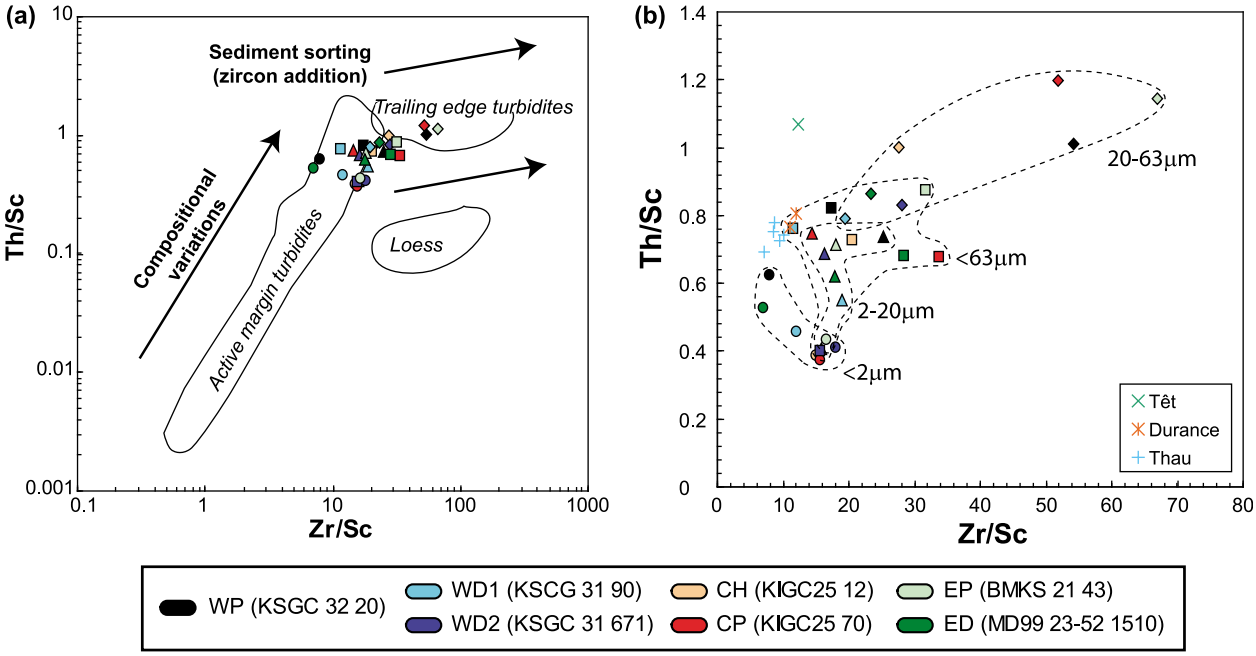

Figure 3. (a) Zr/Sc versus Th/Sc of the Gulf of Lions sediment samples. Also represented are active margin turbidite samples, trailing edge turbidite samples, and loess samples (modified from *Cole et al.* [2009]). Data from *McLennan* [1993, 2001] and *McLennan et al.* [1990]. (b) Zoom on the Gulf of Lions sediments and terrestrial samples. The various grain size fractions are easily identifiable. The coarse silt fractions (20–63 μm) show elevated Zr/Sc ratios indicating zircon addition.

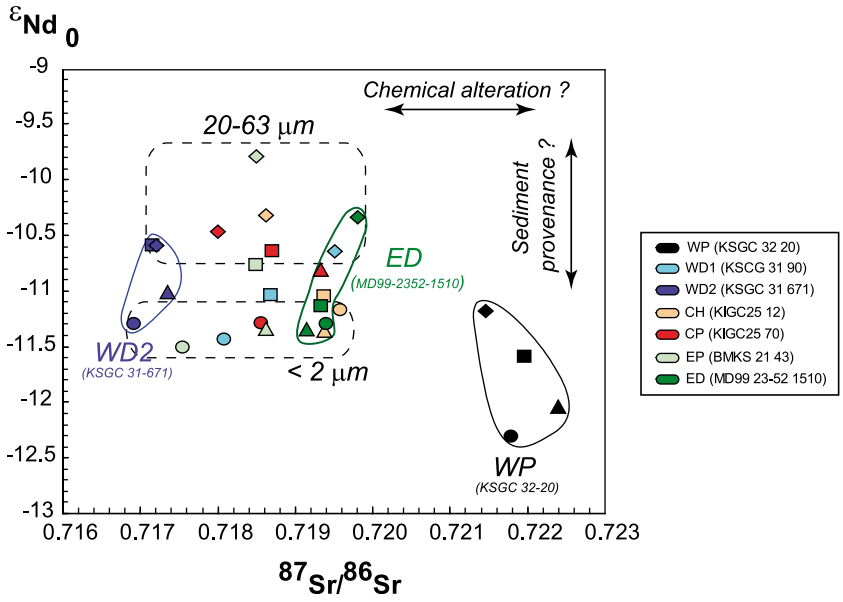

Figure 4. Shown are $^{87}Sr/^{86}Sr$ versus εNd_0 compositions of the Gulf of Lions sediment samples. Two different grain size fractions are highlighted evidencing the variations of Nd isotope compositions with grain size (dashed line). Samples WD2 and ED exhibit the most different Sr isotope compositions. WP is clearly different from the remaining of the Gulf of Lions samples as shown by its Sr and Nd isotope compositions.

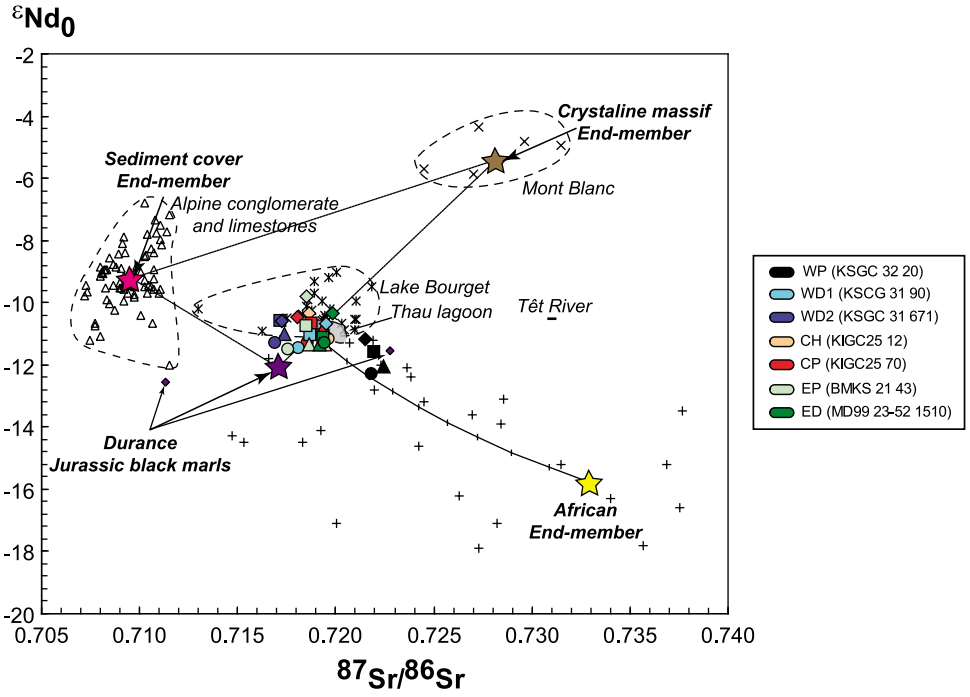

Figure 5. Shown are $^{87}Sr/^{86}Sr$ versus εNd_0 of sediments from the Gulf of Lions together with terrestrial samples. The various end-members are defined as average compositions of samples representing the end-members. Sources of data are as follows. Alpine conglomerates and limestones: *Henry* [1994] and *Henry et al.* [1997]; Mont Blanc and Lake Bourget: *Revel-Rolland et al.* [2005] and *Arnaud et al.* [2008]; Africa: *Grousset et al.* [1998]. The solid line represents a mixing line between the African end-member and the average composition of the Gulf of Lions sediment samples. Ticks represent 10% mixing. As shown by fine dashed lines, sediments from the Gulf of Lions are representative of a mixture between three end-members in the Rhône drainage basin. Additional input of African dust is seen in sample WP.

comparable to REE patterns of our marine sediments samples.

[20] Zr/Sc and Th/Sc ratios of both bulk samples (<63 μm) and fine silts (2–20 μm) are very similar (Figures 3a and 3b). Zr/Sc and Th/Sc ratios vary between 12 to 34 and 0.4 to 0.9, respectively (Figures 3a and 3b). The coarsest fraction is readily identifiable on the Zr/Sc versus Th/Sc ratios diagram: the samples display both higher Zr/Sc (20 to 67) and Th/Sc (0.8 to 1.2) ratios (Figures 3a and 3b). The clay fraction displays the lowest Zr/Sc and Th/Sc ratios (7 to 18 and 0.4 to 0.6, respectively) and is also easily recognized (Figures 3a and 3b).

4.2. Sr and Nd Isotope Data

[21] Sr and Nd isotope compositions of all fractions are reported in Figure 4 and Table 3. Overall, $^{87}Sr/^{86}Sr$ ratios vary between 0.7169 and 0.7198 and εNd_0 vary between −9.8 and −11.5. The only exception to these ranges is sample WP which is distinctively different with $^{87}Sr/^{86}Sr$ and εNd_0 ranging from 0.7215 and 0.7224 and −11.2 to −12.3, respectively (Table 3 and Figure 4). Within the remaining samples, and although variations are not huge, it can be seen that Nd isotope compositions of the clay fractions are, on average, less radiogenic than the coarse silt fractions (εNd_0 = −11.3 ± 0.1 and −10.4 ± 0.3, respectively, Figure 4). On the contrary, the Sr isotope compositions of the various grain sizes are within the same range (Figure 4). Two samples are, however, significantly different one from the other: one distal sample from the western area (WD2, KSGC-31-671, Figure 4) has the lowest $^{87}Sr/^{86}Sr$ ratios (between 0.716921 ± 0.000003 and 0.717348 ± 0.000003, Table 3); and the distal sample from the eastern area (ED, MD99-2352-1510, Figure 4) has the most radiogenic composition (between 0.719147 ± 0.000003 and 0.719796 ± 0.000003, Table 3 and Figure 4). The sample recovered from the Têt River is characterized by an elevated $^{87}Sr/^{86}Sr$ ratio (0.731032 ± 0.000003) and a εNd_0 of −10.6 (Table 4 and Figure 5). Both samples from the Durance have very negative εNd_0 but their Sr isotope compositions are very different (0.711343 ± 0.000003 and 0.722783 ± 0.000003, Table 4 and Figure 5). Sr and Nd isotope composi-

tions of all samples from the Thau lagoon are very homogeneous with an average εNd_0 of -10.9 ± 0.18 and an average $^{87}Sr/^{86}Sr$ ratio of 0.719707 ± 0.00059 (Table 4 and Figure 5).

5. Discussion

5.1. Geochemical Variations With Grain Size

[22] Elevated Zr/Sc ratios in the coarse silt fraction can be explained by the enrichment in heavy mineral (zircon) within this fraction, which will increase the Zr content compared to other immobile elements such as Sc [*McLennan*, 1993; *Taylor and McLennan*, 1985] (Figure 3). The zircon enrichment may also be seen in some of the REE patterns, where coarser silt fractions display increased HREE ratios compared to the other grain size fractions (Figure 2a). Increased Th/Sc ratios in the coarse fraction, compared to clay fractions, can also be related to the presence of heavy minerals such as monazite. Microscopic examination of these fractions further confirms these hypotheses as garnet is absent in the coarse silts and both zircon and monazite were identified.

[23] Although it is often observed that no differences in Nd isotope compositions are seen between grain size fractions, this is not the case in our data set where we have a clear difference between the finest and the coarsest fractions (Figure 4). In fact, previous studies have already reported such variations [*Innocent et al.*, 2000; *Revel et al.*, 1996]. Indeed, the clay fractions (<2 μm) have systematically more negative εNd_0 than the coarse silt fractions (20–63 μm). The minimum difference is seen in sample WD2 with 0.7 epsilon units and the maximum in sample EP with 1.7 epsilon units. As these differences are much higher than analytical errors on Nd isotopic analyses (±0.3 epsilon unit during the course of measurements), we therefore consider these variations as significant. As no well-known secondary mineral can fractionate Sm and Nd, it is unlikely that εNd_0 variations are related to modification of erosion or weathering levels and, they must be related to sediment provenance. Less radiogenic Nd isotope composition may points to an enhanced influence of "older" material in the clay fraction in comparison to the coarse silt fraction. Inputs from two potential candidates could produce more negative εNd_0: dusts from North Africa, derived from erosion of old continental craton, or, easily erodible lithologies such as Jurassic black shales from the Durance watershed (Figures 1 and 5). If African dusts were added, not only the εNd_0 would be more negative but also the $^{87}Sr/^{86}Sr$ ratios would be increased. This is the case only for sample WP, which will be discussed later on, but not for the other samples (Figure 4). Therefore, we suggest that changes in the Nd isotope compositions of the clay fraction are related to input from Jurassic black shales. The coarse silt fractions have less negative εNd_0 values, which is consistent with an enhanced influence of coarser particles originating from crystalline massif (Figures 4 and 5). We propose that particles from Jurassic black marls, from the Durance watershed, are over-represented in the clay fractions, whereas particles from crystalline massif are over-represented in the coarse silts. Variations of εNd_0 between the grain size fractions would therefore be related to a differential sampling of sources. Another argument is that sample EP, which is located next to the Rhône River mouth (Figure 1), displays both the largest difference in εNd_0 between the clay and the silt fraction and the less negative εNd_0 for the coarse silt fraction (−9.8, Table 3) whereas sample WD2, which is far away from the river, displays the smallest variation. Indeed, it is likely that sediments will be better homogenized in the western area than in the eastern area as they are transported via currents over long distance. It is also likely that coarse particles, originating from erosion of the crystalline massif, will be more represented closer to the drainage basin mouth.

[24] We conclude, following previous studies [*Bouchez et al.*, 2011; *Derry and France-Lanord*, 1996; *Innocent et al.*, 2000], that it is critical to carefully choose which grain size fractions are considered in sediment studies. Our data indicate that analyzing and comparing various grain size fractions is essential for sediment provenance studies and such an approach can be used as a complementary tool to examine variable influences from different sources.

5.2. Potential Sources Compositions, Sediment Provenance, and Chemical Weathering

[25] Since early studies it is suggested that most sediment deposited in the Gulf of Lions have been transported through the Rhône River system [*Aloïsi*, 1986]. Calculations of present mass deposition rates highlight the spatial variability of sediment deposition. They are highest in the immediate vicinity of the Rhône River mouth ($4 \pm 2.5\ 10^6$ T yr^{-1}) and decrease rapidly westward ($1.4 \pm 0.2\ 10^6$ T yr^{-1})

[*Durrieu De Madron et al.*, 2000]. However, local sediment input from the Pyrenees rivers can also be important in the western part of the Gulf of Lions, especially during floods. It has been shown that short-term processes, such as floods, may lead to significant sediment discharge from those small, event-dominated, rivers [*Guillén et al.*, 2006]. For example, a major flood event in December 2003 led to the discharge of 2×10^4 T of sediment by the Têt River [*Guillén et al.*, 2006]. It seems therefore important to discriminate between the different potential sources areas, especially for samples in the western part of the Gulf of Lions located close to these river systems.

[26] To determine the provenance of sediments, we compared their geochemical compositions with those of potential source areas. However, it can be seen from the REE patterns (Figure 2) and from trace elements (Figure 3) that distinguishing between the different sources is very difficult as they have fairly similar elemental compositions. Therefore, studying the provenance of sediments from REE and trace elements alone is, in this context, almost impossible as already shown by other studies [*Clift et al.*, 2008].

[27] Apart from the most proximal sample from the western area (WP), which is discussed separately, bulk sediments from the Gulf of Lions show a fairly restricted range of Sr and Nd isotope compositions (Figure 5). Their compositions can be explained by a combination of three distinct main sources: the crystalline end-member, the Cretaceous to Cenozoic sediment cover end-member and the Jurassic black marl end-member from the Durance watershed (Tables 3 and 4, Figure 5). Isotope compositions from the Thau lagoon samples display similar compositions and the potential influence of the Hérault River system is therefore almost impossible to assess with this data set (Tables 3 and 4 and Figure 5). However, given the geographical location of samples from the eastern part of the Gulf of Lions (EP and ED, Figure 1 and Table 1), far away from the Hérault River estuary, and the westward circulation of the Liguro-Provençal Current, it is likely that its influence is minimal. Similarly, sample from the Têt River is clearly distinguished from samples of the Gulf of Lions by its Sr concentration and isotope composition (Tables 3 and 4 and Figure 5). As samples from the western part (WD1 and WD2, Table 1 and Figure 5) do not show elevated $^{87}Sr/^{86}Sr$ compared to the remaining of the samples, we can infer that input from this river system is not significant. However, we note that we have very few analyses of these small river systems and further work is needed for a more extensive characterization.

[28] Finally, we can conclude that samples from the Gulf of Lions, either from the western part or the eastern part, originated from the Rhône River drainage basin, with the exception of sample WP, discussed in the following paragraph. These sediments are therefore mainly produced by the erosion of the Alps and surrounding areas. At this stage it is however still difficult to assess exactly the relative influence of each unit as the Jurassic black marl end-member is not well defined and further analyses from this watershed are necessary.

[29] The proximal sample from the western area (WP) is characterized by more negative εNd_0 and more radiogenic $^{87}Sr/^{86}Sr$ (Figures 4, 5, and 6). Such a difference points to an input of older material but, in contrast to the previous section, this affects all grain size fractions. It also influences both Nd and Sr isotope compositions and this suggests an influence of aeolian dust particles as already reported in numerous studies [*Bout-Roumazeilles et al.*, 2007; *Erel and Torrent*, 2010; *Guerzoni et al.*, 1997; *Moreno et al.*, 2002]. Moreover, palygorskite, which is typical of North African material, is transported by winds and has been described in various locations of the Mediterranean Sea [*Bout-Roumazeilles et al.*, 2007] and the Gulf of Lions [*Van Welden*, 2004]. When reporting the $^{87}Sr/^{86}Sr$ ratios as a function of Sr concentrations (Figure 6), it is clear that the aeolian particles originated from the north and western part of Africa (mainly Mauritania and Mali). Furthermore, such a location is consistent with air masses back-calculated trajectories (Figure 6) [*Grousset and Biscaye*, 2005]. The Sr and Nd isotope compositions of sample WP are influenced by a maximum input of ~20% of North African material (Figures 5 and 6). This is largely consistent with previous studies estimating dust inputs ranging from 10 to 50% in the case of deep sea sedimentation [*Bout-Roumazeilles et al.*, 2007; *Guerzoni et al.*, 1997] or up to 50% in the case of soils [*Erel and Torrent*, 2010; *Yaalon*, 1997]. Available information on KSGC32 core indicates a sedimentation rate of about 40 cm/kyr and a dry density for the sediment of 1.24 g/cm^3. The calculated mass accumulation rate would therefore be about 500 g/m^2/yr. If a maximum input of 20% is taken for aeolian particles, this would represent about 100 g/m^2/yr, which is high but still consistent with fluxes reported in the literature in Mediterranean areas. For example, *Pye* [1992] reports fluxes ranging from 10 to 100 g/m^2/yr (Crete), *Loÿe-*

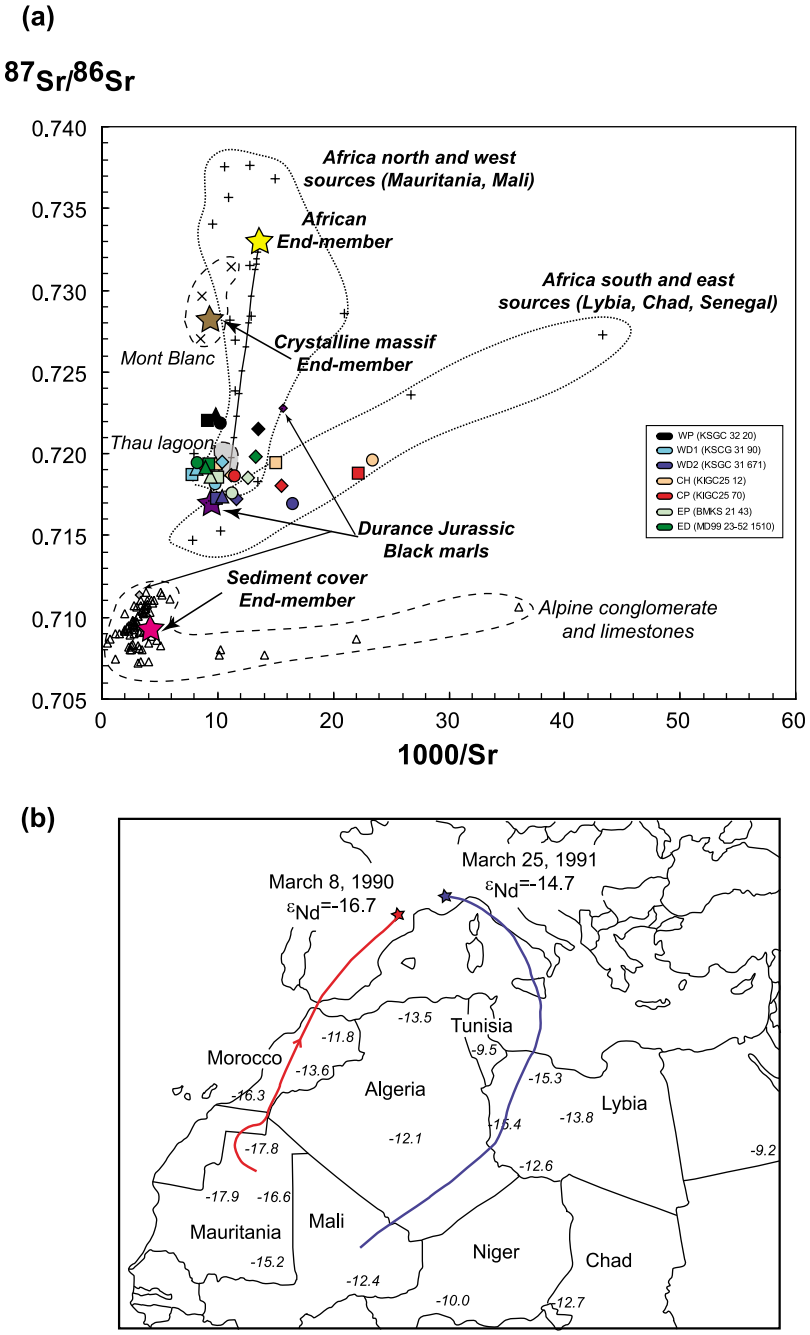

Figure 6. (a) Shown are 1000/Sr versus $^{87}Sr/^{86}Sr$ of sediment samples from the Gulf of Lions. The same end-members as in Figure 5 are represented. Sr concentrations allow distinguishing between a north-west and a south-east origin for the Aeolian inputs. (b) Reconstructed air mass back trajectory of two dust deposition episodes in the French Alps (blue line) and in the Pyrenees mountains (red line). Numbers in italics represents εNd_0 values obtained on North African sand deposits. Adapted from *Grousset and Biscaye* [2005].

Pilot and Martin [1996] from 4 to 26 g/m^2/yr in Corsica and *Guerzoni et al.* [1997] between 30 and 90 g/m^2/yr in the Rhône region.

[30] The amount and variability of chemical weathering is difficult to assess in our data set because this information is somewhat obscured, by the source heterogeneity, as well as variability between grain size fractions. However, some variations within the $^{87}Sr/^{86}Sr$ ratios of our samples can be confidently related to variable intensities of

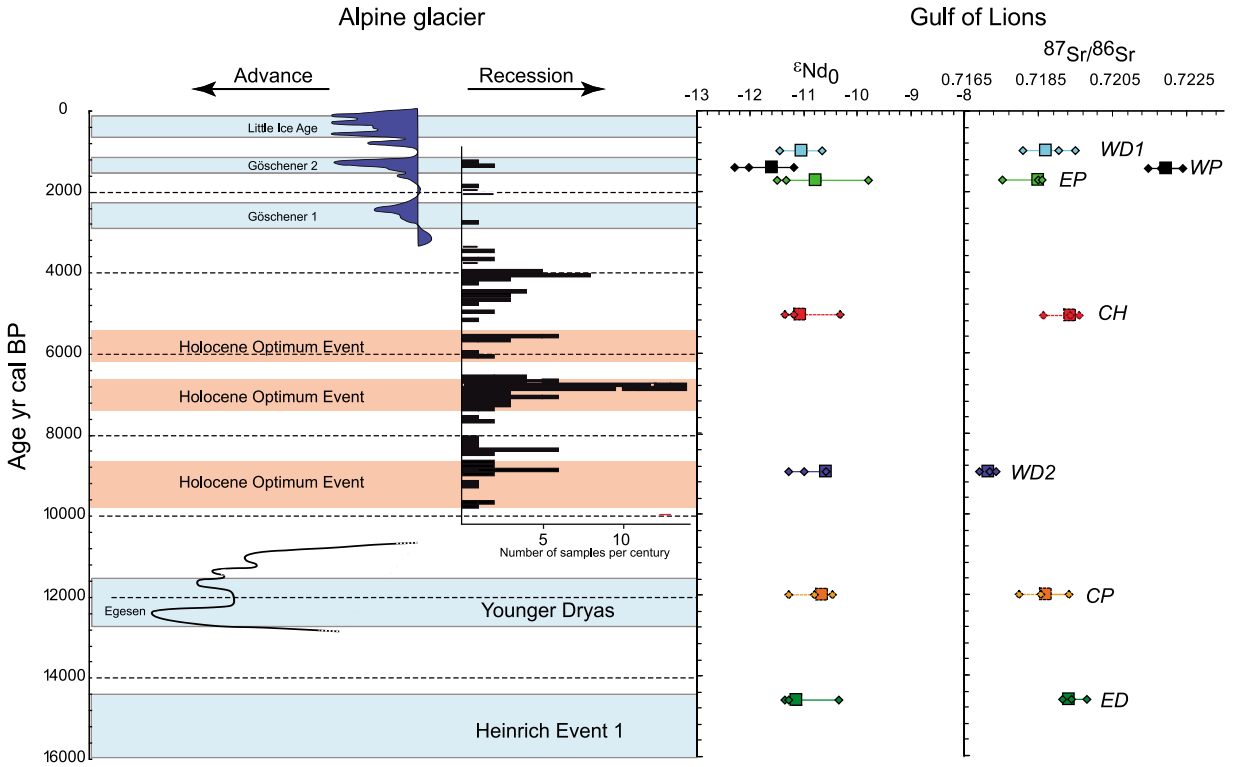

Figure 7. Synthesis of glacier advances and recessions main episodes in the French Alps through the last 16ka Cal BP using data from *Holzhauser et al.* [2005], *Ivy-Ochs et al.* [2009], and *Joerin et al.* [2006, 2008]; εNd_0 and $^{87}Sr/^{86}Sr$ ratios of samples analyzed in this study as a function of their calculated or estimated ages. Error bars on ages are smaller than data points for samples WD1, WD2, WP, EP, and ED. Samples CH and CP are represented with dashed lines because their ages are only estimated. They were positioned arbitrarily at the middle of their age range estimate. Squares represent bulk samples, and diamonds represent the separated grain size fractions.

chemical alteration. Based on the concept of partial dissolution of minerals with high $^{87}Sr/^{86}Sr$ ratios such as clays or mica, high degree of chemical weathering lead to lower bulk sediment $^{87}Sr/^{86}Sr$ ratios [*Blum and Erel*, 1997; *Bullen et al.*, 1997; *Clift et al.*, 2008; *Cole et al.*, 2009; *Colin et al.*, 2006; *Taylor et al.*, 2000]. On the contrary, Nd isotope compositions do not change with variable intensity of chemical weathering. These Sr-Nd relationships are mostly seen in our data set between one distal sample from the western area (WD2) and the distal sample from the eastern area (ED) (Figure 4). Both samples have similar εNd_0 (independently of which grain size fraction is considered) but have different $^{87}Sr/^{86}Sr$ ratios suggesting that sediments originated from the same sources but with variable intensity of chemical weathering. Decrease of mobile elements Cs and Sr compared to immobile element Sc also suggest that sample WD2 formed during an episode of more intense chemical weathering compared to sample ED. However, we must recognize that source versus weathering relationships between these samples are highly complicated and a complete study of separated mineral isotope composition would be necessary to establish a full Sr mass balance budget and understand the role of biotite weathering on the potential release of radiogenic Sr during alteration processes [*Pett-Ridge et al.*, 2009].

5.3. Comparison With Paleoclimatic and Paleoenvironment Reconstructions

[31] We finally compared our interpretations with published paleoenvironmental and paleoclimatic reconstructions (Figure 7). The goal here is not to perform a detailed climate reconstruction, because our sampling has a far too low resolution.

[32] Within the Alps area, the known cold events, from Heinrich event 1 to the Little Ice Age, are well characterized by large glacier advances, with a maximum at about 12.5 ka Cal BP [*Ivy-Ochs et al.*, 2009]. Large glacier recession episodes took place from early Holocene to ~5000 yr Cal BP. These episodes are reported as Holocene Optimum Events

(HOE) and indicate warmer conditions [*Joerin et al.*, 2008, 2006]. Although our sampling is very sparse, some conclusions can be proposed. First, despite numerous climatic oscillations through the Holocene, εNd_0 of our samples remained fairly constant. This is the case either for samples from the eastern, western or central areas in the Gulf of Lions. This may indicate that all samples originated from the same source, which is the Rhône river watershed. We can therefore conclude that sediments provided by the Rhône river system largely dominated sedimentation in the area at least since 16 ka cal BP. Second, and although additional work is needed to confirm this interpretation, there is good consistency between our interpretation of $^{87}Sr/^{86}Sr$ ratios, as a proxy for chemical alteration intensity, and reconstructed climatic conditions. Hence, sample which displays the lowest $^{87}Sr/^{86}Sr$ ratio (WD2, higher degree of chemical alteration) was formed during a Holocene Optimum Event, while the sample with the highest $^{87}Sr/^{86}Sr$ ratio (ED, low degree of chemical alteration) was formed during cold Heinrich Event 1 (Figure 7).

6. Conclusion

[33] The main conclusions of this work are as follows:

[34] 1. Elemental and isotopic compositions of sediments vary as a function of grain size. The coarse silt fraction (20–63 μm) is enriched in heavy minerals such as zircon. Hence, their Zr/Sc ratios are higher than in the other grain size fractions. Nd isotope compositions are also fractionated with grain size. The clay fractions (<2 μm) have more negative εNd_0 that reflect an enhanced contribution of old and fine Jurassic black marls from the Durance watershed. The coarse silt fractions (20–63 μm) have less negative εNd_0 that reflect an enhanced contribution from the Alps crystalline massif. Hence, comparing several grain size fractions can be a very valuable tool in sediment provenance studies.

[35] 2. Sediments deposited in both in the western, eastern or central part of the Gulf of Lions originated from the Rhône watershed. The influence of Pyrenean rivers seems minor in our samples and is not important enough to affect the elemental and isotopic compositions of sediments. Our results also suggest that the overall composition of the Rhône river sediment has not drastically changed since 16 ka cal BP. Only a proximal sample from the western area shows different Sr and Nd isotope compositions that are interpreted as reflecting an input of dust material from northwestern Africa.

[36] 3. When comparing our data to published paleoenvironmental and paleoclimate reconstructions from the French Alps there is a good consistency between our interpretations of Sr isotope compositions, as reflecting conditions of weathering, with known climate fluctuations. It should be noticed however that our sampling is sparse and additional work is needed to confirm this interpretation.

Acknowledgments

[37] This work was supported by Ifremer and French CNRS through funding of SR. Danièle Hureau-Mazaudier, Claire Bassoullet, and Philippe Nonnotte are greatly thanked for their precious help in the geochemistry lab at the Pôle de Spectrométrie Océan in Brest, France. We also thank captains and crews of R/V *Marion Dufresne* and *Le Suroît* for the acquisition of data during cruises Images 5, GMO-Carnac, and Beachmed. N. Thouveny, M. Voisset, and C. Satra, who led these cruises, are also thanked. The French Agence Nationale de la Recherche is thanked for financial support within project Sesame (ANR, contract NT05-3-42040). Associate Editor Louis Derry is warmly thanked for his careful and very constructive comments and advices that greatly improved the quality of the manuscript. Two anonymous reviewers are also thanked for critical and constructive comments.

References

Aloïsi, J. C. (1986), Sur un modele de sedimentation deltaique: Contribution a la connaissance des marges passive, 162 pp., Univ. de Perpignan, Perpignan, France.

Anderson, S. P., et al. (1997), Chemical weathering in glacial environments, *Geology*, *25*, 399–402, doi:10.1130/0091-7613(1997)025<0399:CWIGE>2.3.CO;2.

Arnaud, F., et al. (2008), The Holocene geochemical fingerprint of outer Alps denudation, *Geochim. Cosmochim. Acta*, *72*, A33.

Barrat, J. A., et al. (1996), Determination of rare earth element in sixteen silicate reference samples by ICP-MS after Tm addition and ion exchange separation, *Geostand. Newsl.*, *20*, 133–139, doi:10.1111/j.1751-908X.1996.tb00177.x.

Bayon, G., et al. (2002), An improved method for extracting marine sediment fractions and its application to Sr and Nd isotopic analysis, *Chem. Geol.*, *187*, 179–199, doi:10.1016/S0009-2541(01)00416-8.

Bayon, G., et al. (2009), Determination of rare earth elements, Sc, Y, Zr, Ba, Hf and Th in geological samples by ICP-MS after Tm addition and alkaline fusion, *Geostand. Geoanal. Res.*, *33*, 51–62.

Baztan, J., et al. (2005), Axial incision, the key to understand submarine canyon evolution (in the western Gulf of Lion), *Mar. Pet. Geol.*, *22*, 805–826, doi:10.1016/j.marpetgeo.2005.03.011.

Beaudouin, C., et al. (2007), Vegetation dynamics in southern France during the last 30 ky BP in the light of marine pal-

ynology, *Quat. Sci. Rev.*, *26*, 1037–1054, doi:10.1016/j.quascirev.2006.12.009.
Berné, S., and C. Gorini (2005), The Gulf of Lions: An overview of recent studies within the French "Margins" programme, *Mar. Pet. Geol.*, *22*, 691–693, doi:10.1016/j.marpetgeo.2005.04.004.
Berné, S., et al. (2007), Late Glacial to Preboreal sea-level rise recorded by the Rhône deltaic system (NW Mediterranean), *Mar. Geol.*, *245*, 65–88, doi:10.1016/j.margeo.2007.07.006.
Bickle, M. J., et al. (2005), Relative contributions of silicate and carbonate rocks to riverine Sr fluxes in the headwaters of the Ganges, *Geochim. Cosmochim. Acta*, *69*, 2221–2240, doi:10.1016/j.gca.2004.11.019.
Blum, J. D., and Y. Erel (1997), Rb-Sr isotope systematics of a granitic soil chronosequence: The importance of biotite weathering, *Geochim. Cosmochim. Acta*, *61*, 3193–3204, doi:10.1016/S0016-7037(97)00148-8.
Bouchez, J., et al. (2011), Grain size control of river suspended sediment geochemistry: Clues from Amazon River depth profile, *Geochem. Geophys. Geosyst.*, *12*, Q03008, doi:10.1029/2010GC003380.
Bout-Roumazeilles, V., et al. (2007), Connection between south Mediterranean climate and North African atmospheric circulation during the last 50,000 yr BP North Atlantic cold events, *Quat. Sci. Rev.*, *26*, 3197–3215, doi:10.1016/j.quascirev.2007.07.015.
Braun, J.-J., et al. (2005), Present weathering rates in a humid tropical watershed: Nsimi, South Cameroon, *Geochim. Cosmochim. Acta*, *69*, 357–387, doi:10.1016/j.gca.2004.06.022.
Bullen, T., et al. (1997), Chemical weathering of a soil chronosequence on granitoid alluvium: II. Mineralogic and isotopic constraints on the behavior of strontium, *Geochim. Cosmochim. Acta*, *61*, 291–306, doi:10.1016/S0016-7037(96)00344-4.
Clift, P. D., et al. (2008), Evolving east Asian river systems reconstructed by trace element and Pb and Nd isotope variations in modern and ancient Red River-Song Hong sediments, *Geochem. Geophys. Geosyst.*, *9*, Q04039, doi:10.1029/2007GC001867.
Cole, J. M., et al. (2009), Contrasting compositions of Saharan dust in the eastern Atlantic Ocean during the last deglaciation and African Humid Period, *Earth Planet. Sci. Lett.*, *278*, 257–266, doi:10.1016/j.epsl.2008.12.011.
Colin, C., et al. (2006), Evolution of weathering patterns in the Indo-Burman Ranges over the last 280 kyr: Effects of sediment provenance on 87Sr/86Sr ratios tracer, *Geochem. Geophys. Geosyst.*, *7*, Q03007, doi:10.1029/2005GC000962.
Derry, L. A., and C. France-Lanord (1996), Neogene Himalayan weathering history and river $^{87}Sr/^{86}Sr$: Impact on the marine Sr record, *Earth Planet. Sci. Lett.*, *142*, 59–74, doi:10.1016/0012-821X(96)00091-X.
Dufois, F. (2008), Modélisation du transport particulaire dans le Golfe du Lion en vue d'une application au devenir des traceurs radioactifs issus du Rhône, 409 pp., Univ. su Sud Toulon-Var, Toulon, France.
Durrieu De Madron, X., et al. (2000), Particulate matter and organic carbon budgets for the Gulf of Lions (NW Mediterranean), *Oceanol. Acta*, *23*, 717–730, doi:10.1016/S0399-1784(00)00119-5.
Eisenhauer, A., et al. (1999), Grain size separation and sediment mixing in Arctic Ocean sediments: Evidence from the strontium isotope systematic, *Chem. Geol.*, *158*, 173–188, doi:10.1016/S0009-2541(99)00026-1.
Erel, Y., and J. Torrent (2010), Contribution of Saharan dust to Mediterranean soils assessed by sequential extraction and Pb and Sr isotopes, *Chem. Geol.*, *275*, 19–25, doi:10.1016/j.chemgeo.2010.04.007.
Galy, A., and C. France-Lanord (1999), Weathering processes in the Ganges-Brahmaputra basin and the riverine alkalinity budget, *Chem. Geol.*, *159*, 31–60, doi:10.1016/S0009-2541(99)00033-9.
Galy, V., et al. (2010), Sr-Nd-Os evidence for a stable erosion regime in the Himalaya during the past 12 Myr, *Earth Planet. Sci. Lett.*, *290*, 474–480, doi:10.1016/j.epsl.2010.01.004.
Goldstein, S. L., and R. K. O'Nions (1981), Nd and Sr relationships in pelagic clays and ferromanganese deposits, *Nature*, *292*, 324–327, doi:10.1038/292324a0.
Goldstein, S. L., et al. (1984), A Sm-Nd isotopic study of atmospheric dusts and particulates from major river systems, *Earth Planet. Sci. Lett.*, *70*, 221–236, doi:10.1016/0012-821X(84)90007-4.
Gorini, C., et al. (1993), Contribution to the structural and sedimentary history of the Gulf of Lions (western Mediterranean) from the ECORS profiles, industrial seismic profiles and well data, *Bull. Soc. Geol. Fr.*, *164*, 353–363.
Grousset, F. E., and P. E. Biscaye (2005), Tracing dust sources and transport patterns using Sr, Nd and Pb isotopes, *Chem. Geol.*, *222*, 149–167, doi:10.1016/j.chemgeo.2005.05.006.
Grousset, F. E., et al. (1988), Neodymium isotopes as tracers in marine sediments and aerosols: North Atlantic, *Earth Planet. Sci. Lett.*, *87*, 367–378, doi:10.1016/0012-821X(88)90001-5.
Grousset, F. E., et al. (1998), Saharan wind regimes traced by the Sr-Nd isotopic composition of the tropical Atlantic sediments: Last glacial maximum vs. today, *Quat. Sci. Rev.*, *17*, 395–409, doi:10.1016/S0277-3791(97)00048-6.
Gueguen, E. (1995), La Méditerranée Occidentale: Un véritable océan (Genesis of the western Mediterranean): Exemple de segmentation des marges et de hiatus cinématiques. Implications sur les processus d'amincissement crustal, 281 pp., Univ. de Bretagne Occidentale, Brest, France.
Guerzoni, S., et al. (1997), Saharan dust inputs to the western Mediterranean Sea: Depositional patterns, geochemistry and sedimentological implications, *Deep Sea Res., Part II*, *44*, 631–654, doi:10.1016/S0967-0645(96)00096-3.
Guillén, J., et al. (2006), Sediment dynamics during wet and dry storm events on the Têt inner shelf (SW Gulf of Lions), *Mar. Geol.*, *234*, 129–142, doi:10.1016/j.margeo.2006.09.018.
Henry, P. (1994), Dénudation précoce d'une chaîne et croissance crustale, 156 pp, Univ. de Nancy 1, Nancy, France.
Henry, P., et al. (1997), The erosion of the Alps: Nd isotopic and geochemical constraints on the sources of the peri-Alpine molasse sediments, *Earth Planet. Sci. Lett.*, *146*, 627–644, doi:10.1016/S0012-821X(96)00252-X.
Holzhauser, H., et al. (2005), Glacier and lake-level variations in west-central Europe over the last 3500 years, *Holocene*, *15*, 789–801, doi:10.1191/0959683605hl853ra.
Hughen, K. A., et al. (2004), Marine04 Marine radiocarbon age calibration, 26–0 ka BP, *Radiocarbon*, *46*, 1059–1086.
Innocent, C., et al. (2000), Sm-Nd isotope systematics in deep-sea sediments: Clay-size versus coarser fractions, *Mar. Geol.*, *168*, 79–87, doi:10.1016/S0025-3227(00)00052-9.
Ivy-Ochs, S., et al. (2009), Latest Pleistocene and Holocene glacier variations in the European Alps, *Quat. Sci. Rev.*, *28*, 2137–2149, doi:10.1016/j.quascirev.2009.03.009.
Jacobsen, S. B., and G. J. Wasserburg (1980), Sm-Nd isotopic evolution of chondrites, *Earth Planet. Sci. Lett.*, *50*, 139–155, doi:10.1016/0012-821X(80)90125-9.
Jeong, G. Y., et al. (2006), Rb-Sr and K-Ar systems of biotite in surface environments regulated by weathering processes with implications for isotopic dating and hydrological cycles

of Sr isotopes, *Geochim. Cosmochim. Acta*, *70*, 4734–4749, doi:10.1016/j.gca.2006.07.012.
Joerin, U. E., et al. (2006), Multicentury glacier fluctuations in the Swiss Alps during the Holocene, *Holocene*, *16*, 697–704, doi:10.1191/0959683606hl964rp.
Joerin, U. E., et al. (2008), Holocene optimum events inferred from subglacial sediments at Tschierva Glacier, eastern Swiss Alps, *Quat. Sci. Rev.*, *27*, 337–350, doi:10.1016/j.quascirev.2007.10.016.
Jouet, G. (2007), Enregistrements stratigraphiques des cycles climatiques et glacio-eustatiques du Quaternaire terminal, Modélisations de la marge continentale du Golfe du Lion, Univ. de Bretagne Occidentale, Brest, France.
Jung, S. J. A., et al. (2004), Stepwise Holocene aridification in NE Africa deduced from dust-borne radiogenic isotope records, *Earth Planet. Sci. Lett.*, *221*, 27–37, doi:10.1016/S0012-821X(04)00095-0.
Lee, S.-G., et al. (2008), Rare earth element geochemistry and Nd isotope composition of stream sediments, south Han River drainage basin, Korea, *Quat. Int.*, *176–177*, 121–134, doi:10.1016/j.quaint.2007.05.012.
Lofi, J., et al. (2003), Plio-Quaternary prograding clinoform wedges of the western Gulf of Lion continental margin (NW Mediterranean) after the Messinian Salinity Crisis, *Mar. Geol.*, *198*, 289–317, doi:10.1016/S0025-3227(03)00120-8.
Loÿe-Pilot, M., and J. Martin (1996), Saharan dust input to the western Mediterranean: An eleven years record in Corsica, in *The Impact of Desert Dust Across the Mediterranean*, edited by S. Guerzoni and R. Chester, pp. 191–199, Kluwer Acad., Dordrecht, Netherlands.
Mahoney, J. B. (2005), Nd and Sr isotopic signatures of fine-grained clastic sediments: A case study of western Pacific marginal basins, *Sediment. Geol.*, *182*, 183–199, doi:10.1016/j.sedgeo.2005.07.009.
McLennan, S. M. (1993), Geochemical approaches to sedimentation, provenance, and tectonics, *Spec. Pap. Geol. Soc. Am.*, 21–40.
McLennan, S. M. (2001), Relationships between the trace element composition of sedimentary rocks and upper continental crust, *Geochem. Geophys. Geosyst.*, *2*(4), 1021, doi:10.1029/2000GC000109.
McLennan, S. M., et al. (1990), Geochemical and Nd-Sr isotopic composition of deep-sea turbidites: Crustal evolution and plate tectonic associations, *Geochim. Cosmochim. Acta*, *54*, 2015–2050, doi:10.1016/0016-7037(90)90269-Q.
Millot, C. (1999), Circulation in the western Mediterranean Sea, *J. Mar. Syst.*, *20*, 423–442, doi:10.1016/S0924-7963(98)00078-5.
Moreno, A., et al. (2002), Saharan dust transport and high-latitude glacial climatic variability: The Alboran Sea record, *Quat. Res.*, *58*, 318–328, doi:10.1006/qres.2002.2383.
Najman, Y. (2006), The detrital record of orogenesis: A review of approaches and techniques used in the Himalayan sedimentary basins, *Earth Sci. Rev.*, *74*, 1–72.
Naughton, F., et al. (2009), Wet to dry climatic trend in north-western Iberia within Heinrich events, *Earth Planet. Sci. Lett.*, *284*, 329–342, doi:10.1016/j.epsl.2009.05.001.
Ollivier, P., et al. (2010), Seasonal variations of physical and chemical erosion: A three-year survey of the Rhone River (France), *Geochim. Cosmochim. Acta*, *74*, 907–927, doi:10.1016/j.gca.2009.10.037.
Pett-Ridge, J. C., et al. (2009), Sr isotopes as a tracer of weathering processes and dust inputs in a tropical granitoid watershed, Luquillo Mountains, Puerto Rico, *Geochim. Cosmochim. Acta*, *73*, 25–43, doi:10.1016/j.gca.2008.09.032.
Pin, C., and J. F. Santos Zalduegui (1997), Sequential separation of light rare-earth elements, thorium and uranium by miniaturized extraction chromatography: Application to isotopic analyses of silicate rocks, *Anal. Chim. Acta*, *339*, 79–89, doi:10.1016/S0003-2670(96)00499-0.
Pont, D., et al. (2002), Medium-term changes in suspended sediment delivery to the ocean: Consequences of catchment heterogeneity and river management (Rhône River, France), *Estuarine Coastal Shelf Sci.*, *54*, 1–18, doi:10.1006/ecss.2001.0829.
Popescu, S.-M., et al. (2010), Pliocene and Lower Pleistocene vegetation and climate changes at the European scale: Long pollen records and climatostratigraphy, *Quat. Int.*, *219*, 152–167, doi:10.1016/j.quaint.2010.03.013.
Pye, K. (1992), Aeolian dust transport and deposition over Crete and adjacent parts of the Mediterranean Sea, *Earth Surf. Processes Landf.*, *17*, 271–288, doi:10.1002/esp.3290170306.
Rabineau, M., et al. (2006), Paleo sea levels reconsidered from direct observation of paleoshoreline position during Glacial Maxima (for the last 500,000 yr), *Earth Planet. Sci. Lett.*, *252*, 119–137, doi:10.1016/j.epsl.2006.09.033.
Reimer, P. J., et al. (2004), IntCal04 terrestrial radiocarbon age calibration, *Radiocarbon*, *46*, 1029–1058.
Revel, M., et al. (1996), Grain-size and Sr-Nd isotopes as tracer of paleo-bottom current strength, Northeast Atlantic Ocean, *Mar. Geol.*, *131*, 233–249, doi:10.1016/0025-3227(96)00005-9.
Revel, M., et al. (2010), 100,000 years of African monsoon variability recorded in sediments of the Nile margin, *Quat. Sci. Rev.*, *29*, 1342–1362, doi:10.1016/j.quascirev.2010.02.006.
Revel-Rolland, M., et al. (2005), Sr and Nd isotopes as tracers of clastic sources in Lake Le Bourget sediment (NW Alps, France) during the Little Ice Age: Palaeohydrology implications, *Chem. Geol.*, *224*, 183–200, doi:10.1016/j.chemgeo.2005.04.014.
Révillon, S., and D. Hureau-Mazaudier (2009), Improvements in digestion protocols for trace element and isotope determinations in stream and lake sediment reference materials (JSd-1, JSd-2, JSd-3, JLk-1 and LKSD-1), *Geostand. Geoanal. Res.*, *33*, 397–413, doi:10.1111/j.1751-908X.2009. 00008.x.
Révillon, S., et al. (2008), Linking erosion rates and climatic variations in the Gulf of Lions, France: A geocheinical approach, *Geochim. Cosmochim. Acta*, *72*, A789.
Sánchez Goñi, M. F., et al. (2008), Contrasting impacts of Dansgaard-Oeschger events over a western European latitudinal transect modulated by orbital parameters, *Quat. Sci. Rev.*, *27*, 1136–1151, doi:10.1016/j.quascirev.2008.03.003.
Sierro, F. J., et al. (2009), Phase relationship between sea level and abrupt climate change, *Quat. Sci. Rev.*, *28*, 2867–2881, doi:10.1016/j.quascirev.2009.07.019.
Sioni, S. (1997), Mer Ionienne et Apulie depuis l'ouverture de l'Océan Alpin (Evolution of Ionian Sea and Apulia from alpine oceanic opening), 208 pp., Univ. de Bretagne Occidentale, Brest, France.
Stuiver, M., and P. J. Reimer (1993), Extended 14C database and revised CALIB radiocarbon calibration program, *Radiocarbon*, *35*, 215–230.
Taylor, S. S., and S. M. McLennan (1985), *The Continental Crust: Its Composition and Evolution*, 312 pp., Blackwell Sci., Palo Alto, Calif.

Taylor, S. R., and S. M. McLennan (1995), The geochemical evolution of the continental crust, *Rev. Geophys.*, *33*, 241–265, doi:10.1029/95RG00262.

Taylor, A. S., et al. (2000), Kinetics of dissolution and Sr release during biotite and phlogopite weathering, *Geochim. Cosmochim. Acta*, *64*, 1191–1208, doi:10.1016/S0016-7037(99)00369-5.

Tütken, T., et al. (2002), Glacial-interglacial cycles in Sr and Nd isotopic composition of Arctic marine sediments triggered by the Svalbard/Barents Sea ice sheet, *Mar. Geol.*, *182*, 351–372, doi:10.1016/S0025-3227(01)00248-1.

Van Welden, A. (2004), Variations haute résolution des apports terrigenes dans le Golfe du Lion pendant la dernière période glaciaire: Caractérisation des évènements climatiques rapides, 71 pp., Univ. de Lille, Lille, France.

Verplanck, E. P., et al. (2009), Provenance of Quaternary glacial and glacimarine sediments along the southeast Greenland margin, *Earth Planet. Sci. Lett.*, *286*, 52–62, doi:10.1016/j.epsl.2009.06.012.

Vital, H., and K. Stattegger (2000), Major and trace elements of stream sediments from the lowermost Amazon River, *Chem. Geol.*, *168*, 151–168, doi:10.1016/S0009-2541(00)00191-1.

White, W. M., et al. (1985), Isotope and trace element geochemistry of sediments from the Barbados Ridge-Demerara Plain region, Atlantic Ocean, *Geochim. Cosmochim. Acta*, *49*, 1875–1886, doi:10.1016/0016-7037(85)90082-1.

Yaalon, D. H. (1997), Soils in the Mediterranean region: What makes them different?, *Catena*, *28*, 157–169, doi:10.1016/S0341-8162(96)00035-5.